

Particle reconstruction of volumetric particle image velocimetry with strategy of machine learning

Qi Gao¹ · Qijie Li² · Shaowu Pan³✉ · Hongping Wang² · Runjie Wei² · Jinjun Wang⁴

Abstract Three-dimensional particle reconstruction with limited two-dimensional projects is an underdetermined inverse problem that the exact solution is often difficult to be obtained. In general, approximate solutions can be obtained by optimization methods. In the current work, a practical particle reconstruction method based on convolutional neural network (CNN) is proposed. The proposed technique can refine the particle reconstruction from a very coarse initial guess of particle distribution from any traditional algebraic reconstruction technique (ART) based methods. Compared with available ART-based algorithms, the novel technique makes significant improvements in terms of reconstruction quality and at least an order of magnitude faster with dense particle concentration.

Keywords Particle reconstruction · Volumetric particle image velocimetry · Convolutional neural network

1 Introduction

Particle image velocimetry (PIV) is a widely used technique for measuring velocity fields. With volumetric PIV measurement, complex flows can be investigated regarding to their three-dimensional three-component (3D3C) flow structures. Among all the 3D3C measurement methods, tomographic PIV (Tomo-PIV) proposed by Elsinga et al (2006) has been proved on its success of making accurate measurement with fine spacial resolution under a fairly high particle seeding density of 0.05 ppp (particle per pixel). The key procedure of Tomo-PIV is the particle reconstruction (PR), which is a process of solving inverse projection problem from two-dimensional particle images to 3D intensity distribution of particles. In the original article of Tomo-PIV by Elsinga et al (2006), the multiplicative algebraic reconstruction technique

(MART) based on the maximum entropy criterion was introduced to reconstruct the 3D particle field. Since then, numerous advanced techniques have been developed to optimize the 3D particle reconstruction for improving either accuracy or efficiency, which has been well reviewed by Scarano (2012) and Gao et al (2013). Most available particle reconstruction techniques are based on MART algorithm, such as the spatial filtering MART (SF-MART), which applies a spatial filtering on the reconstructed particle intensity field after each MART iteration (Discetti et al, 2013). SF-MART provides a better reconstruction quality than the traditional MART algorithm, which will be tested and compared with the new technique in the current work.

For the PR problem, with the increase of particle seeding density, the reconstruction quality decreases rapidly due to the issue of ghost particles, which is a fake particle unexpectedly generated at the intersections of light of sight (LOS). Many algorithms were proposed to improve the reconstruction quality under high particle concentration. Worth and Nickels (2008) used multiplicative first guess (MFG) as a precursor to the standard MART approach, which can provide a reasonably accurate solution as initial condition for MART iteration and also accelerate the convergence. Atkinson and Soria (2009) further proposed a multiplicative LOS (MLOS) estimation to determine the possible particle locations without requiring the weighting matrix as MFG. Besides having a good initialization, removal of ghost particles can substantially improve the reconstruction quality. The joint distribution of peak intensity and track length can be used to successfully separate ghost particles and actual particles in certain cases (Elsinga and Tokgoz, 2014). A simulacrum matching-based reconstruction enhancement (SMRE) technique proposed by de Silva et al (2013) utilizes the characteristic shape and size of actual particles to remove ghost particles in the reconstructed intensity field. The Shake-The-Box (STB) approach (Schanz et al, 2014, 2016) uses the known trajectories to predict the particle distribution. The particle locations are consequently corrected by Iterative Reconstruction of Volumetric Particle Distribution (IPR) proposed by Wieneke (2013). STB has a considerable improvement compared to MART in both accuracy and particle concentration. For time-resolved image acquisition, sequential motion tracking enhancement MART (SMTE-MART) proposed by Lynch and Scarano (2015) also produces a time-marching estima-

Q. Gao
School of Aeronautics and Astronautics, Zhejiang University,
Hangzhou, China, 310027

Q. J. Li · H. P. Wang · R. J. Wei
MicroVec. Inc., Beijing, China, 100191

S. W. Pan (✉)
Department of Aerospace Engineering, University of Michigan, Ann
Arbor, MI, 48105
E-mail: Shawnpan@umich.edu

J. J. Wang
Key Laboratory of Fluid Mechanics, Ministry of Education, Beihang
University, Beijing, China, 100191

tion of the object intensity field based on an enhanced guess, which is built upon the object reconstructed at the previous time instant. This method yields superior reconstruction quality and higher velocity field measurement precision when compared with both MART and MTE-MART (Novara et al, 2010). For single volume reconstruction, some new reconstruction schemes were developed. Intensity-enhanced MART (IntE-MART) uses a histogram-based intensity reduction to suppress the intensity of ghosts (Wang et al, 2016). Gesemann et al (2010) solved the volume intensity using a optimization algorithm based on constrained least squares strategies and L1-regularization. Ye et al (2015) proposed a dual-basis pursuit approach for particle reconstruction, which yielded higher reconstruction quality comparing with MART in 2D simulations. In order to reduce the computational time, Bajpayee and Techet (2017) presented a memory-efficient and highly parallelizable method based on a homography fit synthetic aperture refocusing method. Rather than a ‘voxel-oriented’ approach, Ben Salah et al (2018) proposed an ‘object-oriented’ approach called Iterative Object Detection-Object Volume Reconstruction based on Marked Point Process (IOD-OVRMPP) for the reconstruction of a population of 3D objects. The particle position can be directly obtained using this method.

With the development of machine learning in the field of image processing, designing a model based on machine learning to deal with various image-related tasks has become a hot topic. In the past few years, neural networks have begun to be applied to particle image velocimetry. Machine learning has been utilizing to replace traditional cross-correlation for velocity deduction with dense particle seeding (Cai et al, 2019a; Cai et al, 2019b). Recently, a series work has been presented in a conference, ‘13th International Symposium on Particle Image Velocimetry’ (ISPIV 2019, Munich, Germany, July 22-24). For example, Lagemann et al (2019) applied convolutional neural networks (CNN) to PIV and achieved similar effects of traditional cross-correlation algorithms. However, at the moment, most existing works on applying machine learning with PIV are two dimensional while investigation of applying machine learning on particle reconstruction, as a fully three-dimensional application, is still lacking. In this work, we utilize 3D CNN in design a machine learning algorithm for 3D particle reconstruction problem, termed as ‘AI-PR’.

2 Principle of particle reconstruction with machine learning

2.1 Particle reconstruction as inverse problem

We formulate the problem of searching for the particle reconstruction from several projections of the particle field as

inverse problem (Minerbo, 1979). Consider a fixed three dimensional orthogonal coordinate system, $(x, y, z) \in \mathbb{R}^3$, the unknown particle field can be viewed as a continuous source function $f \in C^0(\mathcal{D})$ satisfying,

$$f(x, y, z) \geq 0, \quad \iiint_{\mathcal{D}} f(x, y, z) dx dy dz = 1, \quad (1)$$

where $\mathcal{D} \subset \mathbb{R}^3$ is a compact support of f .

Assuming parallel projection (or point spread function), without loss of generality, a view can be defined as rotation of coordinate system with respect to some certain origin. One can further introduce different translation for cameras but it is ignored in the context for better illustration. The coordinate in the rotated system is $(x', y', z') \in \mathbb{R}^3$ where $x' - y'$ plane is parallel to the projection plane of the view, i.e., z' is parallel to the line of sight, determined by the following relation,

$$\begin{bmatrix} x' & y' & z' \end{bmatrix}^T = \mathbf{T} \begin{bmatrix} x & y & z \end{bmatrix}^T, \quad (2)$$

where the rotation matrix \mathbf{T} specified by three Euler angles α, β, γ is defined as,

$$\mathbf{T} = \begin{bmatrix} \cos \alpha \cos \gamma - \sin \alpha \cos \beta \sin \gamma & -\cos \alpha \sin \gamma - \sin \alpha \cos \beta \cos \gamma & \sin \alpha \sin \beta \\ \sin \alpha \cos \gamma - \cos \alpha \cos \beta \sin \gamma & -\sin \alpha \sin \gamma + \cos \alpha \cos \beta \cos \gamma & -\cos \alpha \sin \beta \\ \sin \beta \sin \gamma & \sin \beta \cos \gamma & \cos \beta \end{bmatrix}. \quad (3)$$

In practice, there are J views, i.e., number of cameras, usually ranging from 4 to 6. For each j -th view, the two dimensional projection field $g_j(x', y')$ is given as,

$$g_j(x', y') = \int_{-\infty}^{\infty} f(\mathbf{T}_j^{-1} \begin{bmatrix} x' & y' & z' \end{bmatrix}^T) dz'. \quad (4)$$

The goal of the inverse problem is to find the source function f , given projection data $\{g_j\}_{j=1}^J$ in the discretized form, i.e., f are pixelized as function dealing with 3D matrix and g_j as 2D images. Unfortunately, it is known to have infinite number of solutions satisfying all the above conditions (Guenther et al, 1974; Huesman, 1977). Most often, additional conditions, e.g., entropy maximization Minerbo (1979), is considered to enforce uniqueness.

2.2 Learning particle reconstruction field via CNN

2.2.1 Physics-informed input features

We consider the initial particle field \mathbf{E}_{MLOS} in Eq. 5 generated by MLOS method as input for the CNN. Because the geometrical optics information, i.e., directions and positions of all the cameras, are embedded, \mathbf{E}_{MLOS} is physics-informed.

$$\mathbf{E}_{\text{MLOS}}(x, y, z) = \prod_{j=1}^J g_j(\tilde{\mathbf{T}} \begin{bmatrix} x & y & z \end{bmatrix}^T), \quad (5)$$

where $\tilde{\mathbf{T}}$ is the first two rows of \mathbf{T} .

2.2.2 Mathematical Formulation of a single Convolutional Layer

To begin with we denote the shape of general multi-channel 3D convolution field as $(N_x \times N_y \times N_z \times Q)$ with last index as the channel.

Now we define the convolution operation with kernel $\mathbf{K} \in \mathbb{R}^{L \times M \times N \times Q \times Q'}$ on multi-channel 3D objects $\mathbf{V} \in \mathbb{R}^{N_x \times N_y \times N_z \times Q}$ with output $\mathbf{Z} \in \mathbb{R}^{N'_x \times N'_y \times N'_z \times Q'}$ as $\mathbf{Z} = c(\mathbf{K}, \mathbf{V}, s)$. Specifically, for index $1 \leq i \leq N'_x$, $1 \leq j \leq N'_y$, $1 \leq k \leq N'_z$, and channel index $1 \leq q' \leq Q'$, combining with zero-padding in Eq. 6 to avoid shrinkage of image size so as to enable deeper neural networks,

$$\tilde{\mathbf{V}}(l, m, n; i, j, k) = \begin{cases} \mathbf{V}_{(i-1)s+l, (j-1)s+m, (k-1)s+n, q} & \text{if } 1 \leq (i-1)s+l \leq N_x \\ & \text{and } 1 \leq (j-1)s+m \leq N_y \\ & \text{and } 1 \leq (k-1)s+n \leq N_z \\ 0 & \text{otherwise} \end{cases}, \quad (6)$$

we have the following general expression for zero-padding convolution operation,

$$\mathbf{Z}_{i,j,k,q'} = c(\mathbf{K}, \mathbf{V}, s)_{i,j,k,p} \quad (7)$$

$$= \sum_{q=1}^Q \sum_{l=\frac{1-L}{2}}^{\frac{L+1}{2}} \sum_{m=\frac{1-M}{2}}^{\frac{M+1}{2}} \sum_{n=\frac{1-N}{2}}^{\frac{N+1}{2}} \tilde{\mathbf{V}}(l, m, n; i, j, k) \mathbf{K}_{l,m,n,q,q'}. \quad (8)$$

After obtaining the output field \mathbf{Z} , an element-wise nonlinear activation function $\sigma(\cdot) : \mathbb{R} \mapsto \mathbb{R}$ is applied on \mathbf{Z} . Finally, the whole process including the nonlinear activation above defined in Eq. 9 is called a *convolutional layer C* without pooling,

$$\mathbf{V}' = \sigma(\mathbf{Z}) = \sigma(c(\mathbf{K}, \mathbf{V}, s)) = C(\mathbf{V}) \in \mathbb{R}^{N'_x \times N'_y \times N'_z \times Q'}. \quad (9)$$

2.2.3 Architecture of AI-PR

Given the definition of a *convolutional layer* above as the building block, the architecture of convolutional neural network is illustrated in Fig. 1. Two major steps are processed to achieve the final particle field. The first step calculates a three-dimensional initial particle field (\mathbf{E}_{MLOS}) from multiple two-dimensional particle images by camera imaging, which is the same as traditional PR algorithms, while MLOS method has been noticed as a very good initial guess of particle field. The second step uses a convolutional neural network to learn the three-dimensional particle field with given input as the initial guess of particle field.

The deep convolutional neural network with 12 layers was built to learn the 3D particle field. The input and output were both $64 \times 64 \times 32 \times 1$. The activation function of the last layer was Sigmoid function, while the other layers used ReLU function. Except the input layer and the output layers, all the rest layers were sizes of $64 \times 64 \times 32 \times 16$ with the Batch normalization method (Ioffe and Szegedy, 2015)

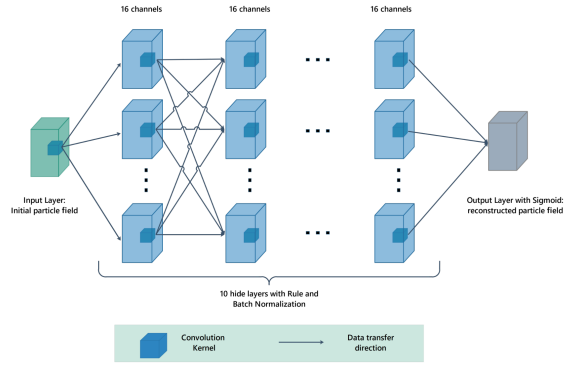


Fig. 1: Schematic diagram of neural network structure

adopted on these layers. The convolution kernel of the input layer was size of $3 \times 3 \times 3 \times 1$, while the other layers had size of kernel as $3 \times 3 \times 3 \times 16$.

In real experiments, it is often impossible to obtain exact locations and intensity distribution of particles from measurement. Hence, synthetic particle field was employed as training and testing data. The synthetic particle fields and their images were generated following typical way that has been widely used for testing PR algorithms. Details can be found in Wang et al (2016) and Ye et al (2015). Four projections of particle fields were calculated from given mapping functions to simulate camera imaging. The initial MLOS field was then computed and prepared as input for the aforementioned 3D CNN.

In order to improve the robustness of the CNN, we considered 20% of the total training particle images biased with Gaussian noises. Different degrees of Gaussian noise were added to the four particle images. Following the typical way of adding noises (Wang et al, 2016; Cai et al, 2019a), the standard deviation σ of the image noise was calculated with levels of $n\sigma$ for PR testing, where n was from 0 to 0.2 with interval of 0.05. It was noticed that the performance of the new algorithm was stable and accurate enough when the size of training examples was over 500. The loss function for training the network was defined as:

$$loss = \frac{\sum_{i=1}^M \text{sum}(\mathbf{F}^{(i)} \times \mathbf{F}_{nm}^{(i)})}{\sum_{i=1}^M \text{sum}(\mathbf{F}^{(i)} - \mathbf{F}_{nm}^{(i)}) + \epsilon}, \quad (10)$$

where \mathbf{F} is the target true tensor, \mathbf{F}_{nm} is the network output tensor, and ϵ is a small value to prevent the denominator from being zero, which was 10^{-3} in the current work. Operator ' \times ' represents the multiplication of the corresponding elements in the matrix, $\text{sum}(\cdot)$ indicates the summation of all elements of the matrix. i is the index of training sample, M is the number of training samples.

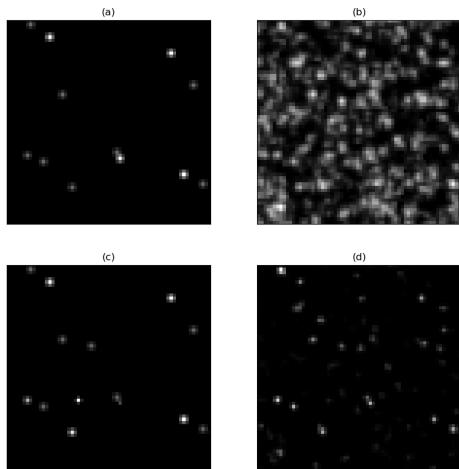


Fig. 2: Cross-sections of particle field, (a) Synthetic field, (b)MLOS field, (c)AI-PR, (d) MART field with 10 iterations.

3 Results and discussions

Since it is difficult to directly test particle reconstruction technique with real experimental data, the AI-PR algorithm was tested with synthetic data. The testing particle fields was generated with the same manner as the training set with size of $780 \times 780 \times 140$. Seeding density was tested from $ppp = 0.05$ to 0.3 with interval of 0.05 . Noise level was tested from $n = 0.05$ to 0.3 with interval of 0.05 . Three traditional PR methods: MLOS, MART with five and ten times iterations, together with proposed method in this work are considered for comparison against each other. All the training and testing were under the framework of TensorflowTM V1.13.1 (Abadi et al, 2016) programmed with Python (www.python.org) and Matlab[®] (MathWorks, Inc.). The computer used was an Intel x99 workstation with one CPU of E5-2696 V4, 64GB DDR4 memory and a RTX2080ti graphics processing unit.

Fig. 2 provides a central cross-sections of a reconstructed particle field with $ppp = 0.15$. It is obvious that MLOS only gives a very coarse initial guess of potential particle location and intensity distribution, while AI-PR and MART can recover better particle fields. Comparing further between AI-PR and MART methods, it is notable that MART generates more ghost particles and has worse intensity distribution than AI-PR does. If the particle shape is looked closer, it can be found that MART-reconstructed particles have more ellipsoid shape, when AI-PR restores the spherical shape better.

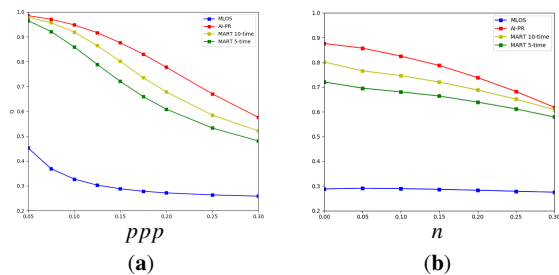


Fig. 3: Quality factor Q of different methods with effects of (a) seeding density and (b) noise levels.

In terms of reconstruction quality, AI-PR shows its superiority to MART methods as shown in Fig. 3. The quality factor Q was utilized for evaluating the accuracy and stability of the new technique, which is the correlation coefficient between the synthetic and reconstructed fields. In Fig. 3a, all the methods were tested without imaging noise. It is shown that AI-PR can recover the particle significantly from MLOS field. It has better Q than MART methods. When ppp researches 0.25 , the Q remains at around 0.7 for AI-PR, while MART-10 reduces below 0.6 . If the effect of noise is parameterized in Fig. 3b at $ppp = 0.15$, the Q reduces with increase of noise level for all methods, but AI-PR has the best stability against the biases.

When the efficiency of the calculation is concerned, the algorithms of MLOS, MART-5, MART-10 and AI-PR costed $512.5s$, $5333.5s$, $9881.5s$, and $524.5s$, respectively. Since AI-PR processing included the computing cost of MLOS and CNN, the actual computing time was only about $12s$. However, it is noticed that the training of CNN costed about 16 hours for 100 epochs and the MART algorithm did not accelerate with GPU in the current work.

4 Conclusions

For the three-dimensional particle reconstruction of volumetric PIV, the new proposed AI-based technique shows its superior advantages of accuracy, efficiency and robustness on recovering particle locations and intensities from 2D particle images over traditional MART-based algorithms. Overall, with its superior accuracy and robustness, we believe AI-PR technique is very promising to apply to more realistic experiments. However, it needs to be noticed that for different experiments with different mapping functions of imaging, AI-PR requires its entire training procedure to learn the rules of projections. Future work could focus on combining calibration of volumetric PIV with AI-PR training, or doing particle reconstruction directly from AI-PR without calibration and additional network training for different experimental cases.

5 Acknowledgements

This work was supported by the National Natural Science Foundation of China (grant No. 91852204, 11721202) and the Fundamental Research Funds for the Central Universities (2019QNA4056).

References

- Abadi M, Barham P, Chen J, Chen Z, Davis A, Dean J, Devin M, Ghemawat S, Irving G, Isard M, Kudlur M, Levenberg J, Monga R, Moore S, Murray DG, Steiner B, Tucker P, Vasudevan V, Warden P, Wicke M, Yu Y, Zheng X (2016) Tensorflow: A system for large-scale machine learning. In: 12th USENIX Symposium on Operating Systems Design and Implementation (OSDI 16), pp 265–283
- Atkinson C, Soria J (2009) An efficient simultaneous reconstruction technique for tomographic particle image velocimetry. *Experiments in Fluids* 47(4):553–568
- Bajpayee A, Techet AH (2017) Fast volume reconstruction for 3d PIV. *Experiments in Fluids* 58(8):95
- Ben Salah R, Alata O, Tremblais B, Thomas L, David L (2018) Tomographic reconstruction of 3d objects using marked point process framework. *Journal of Mathematical Imaging and Vision* 60(7):1132–1149
- Cai S, Zhou S, Xu C, Gao Q (2019a) Dense motion estimation of particle images via a convolutional neural network. *Experiments in Fluids* 60:1–16
- Cai S, Liang J, Gao Q, Xu C, Wei R (2019b) Particle image velocimetry based on a deep learning motion estimator. *IEEE Transactions on Instrumentation and Measurement* pp 1–1
- Discetti S, Natale A, Astarita T (2013) Spatial filtering improved tomographic piv. *Experiments in Fluids* 54(4):1505
- Elsinga GE, Tokgoz S (2014) Ghost hunting—an assessment of ghost particle detection and removal methods for tomographic-PIV. *Measurement Science and Technology* 25(8):084,004
- Elsinga GE, Scarano F, Wieneke B, van Oudheusden BW (2006) Tomographic particle image velocimetry. *Exp Fluids* 41(6):933
- Gao Q, Wang H, Shen G (2013) Review on development of volumetric particle image velocimetry. *Chinese Science Bulletin* 58(36):4541–4556
- Gesemann S, Schanz D, Schröder A, Petra S, Schnörr C (2010) Recasting Tomo-PIV reconstruction as constrained and L1-regularized nonlinear least squares problem. In: 15th Int Symp on Applications of Laser Techniques to Fluid Mechanics
- Guenther R, Kerber C, Killian E, Smith K, Wagner S (1974) Reconstruction of objects from radiographs and the location of brain tumors. *Proceedings of the National Academy of Sciences* 71(12):4884–4886
- Huesman R (1977) The effects of a finite number of projection angles and finite lateral sampling of projections on the propagation of statistical errors in transverse section reconstruction. *Physics in Medicine & Biology* 22(3):511
- Ioffe S, Szegedy C (2015) Batch normalization: Accelerating deep network training by reducing internal covariate shift. *arXiv preprint arXiv:1502.03167*
- Lagemann C, Lagemann K, Schröder W, Klaas M (2019) Deep artificial neural network architectures in PIV applications. In: 13th International Symposium on Particle Image Velocimetry
- Lynch KP, Scarano F (2015) An efficient and accurate approach to MTE-MART for time-resolved tomographic piv. *Experiments in Fluids* 56(3):1–16
- Minerbo G (1979) Ment: A maximum entropy algorithm for reconstructing a source from projection data. *Computer Graphics and Image Processing* 10(1):48–68
- Novara M, Batenburg KJ, Scarano F (2010) Motion tracking-enhanced MART for tomographic PIV. *Measurement Science and Technology* 21(3):035,401
- Scarano F (2012) Tomographic PIV: principles and practice. *Measurement Science and Technology* 24(1):012,001
- Schanz D, Schröder A, Gesemann S (2014) ‘Shake The Box’ - a 4D PTV algorithm: Accurate and ghostless reconstruction of Lagrangian tracks in densely seeded flows. In: 17th International Symposium on Applications of Laser Techniques to Fluid Mechanics
- Schanz D, Gesemann S, Schröder A (2016) Shake-the-box: Lagrangian particle tracking at high particle image densities. *Experiments in Fluids* 57(5):70
- de Silva CM, Baidya R, Marusic I (2013) Enhancing Tomo-PIV reconstruction quality by reducing ghost particles. *Measurement Science and Technology* 24(2):024,010
- Wang H, Gao Q, Wei R, Wang J (2016) Intensity-enhanced mart for tomographic PIV. *Experiments in Fluids* 57(5):87
- Wieneke B (2013) Iterative reconstruction of volumetric particle distribution. *Measurement Science and Technology* 24(2):024,008
- Worth NA, Nickels TB (2008) Acceleration of Tomo-PIV by estimating the initial volume intensity distribution. *Experiments in Fluids* 45(5):847–856
- Ye ZJ, Gao Q, Wang HP, Wei RJ, Wang JJ (2015) Dual-basis reconstruction techniques for tomographic PIV. *Science China Technological Sciences* 58(11):1963–1970